

Search for a New  $B - L Z'$  Gauge Boson with the NA64 Experiment at CERN

Yu. M. Andreev,<sup>1</sup> D. Banerjee,<sup>2</sup> B. Banto Oberhauser,<sup>3</sup> J. Bernhard,<sup>2</sup> P. Bisio,<sup>4,5</sup> V. E. Burtsev,<sup>6</sup> A. Celentano,<sup>4</sup> N. Charitonidis,<sup>2</sup> A. G. Chumakov,<sup>7</sup> D. Cooke,<sup>8</sup> P. Crivelli,<sup>3</sup> E. Depero,<sup>3</sup> A. V. Dermenev,<sup>1</sup> S. V. Donskov,<sup>9</sup> R. R. Dusaev,<sup>7</sup> T. Enik,<sup>6</sup> V. N. Frolov,<sup>6</sup> A. Gardikiotis,<sup>10</sup> S. G. Gerassimov,<sup>11,12</sup> S. N. Gninenko,<sup>1,\*</sup> M. Hösgen,<sup>13</sup> M. Jeckel,<sup>2</sup> V. A. Kachanov,<sup>9</sup> A. E. Karneyeu,<sup>1</sup> G. Kekelidze,<sup>6</sup> B. Ketzer,<sup>13</sup> D. V. Kirpichnikov,<sup>1</sup> M. M. Kirsanov,<sup>1</sup> V. N. Kolosov,<sup>9</sup> S. G. Kovalenko,<sup>14,15</sup> V. A. Kramarenko,<sup>6,16</sup> L. V. Kravchuk,<sup>1</sup> N. V. Krasnikov,<sup>6,1</sup> S. V. Kuleshov,<sup>14,15</sup> V. E. Lyubovitskij,<sup>7,15</sup> V. Lysan,<sup>6</sup> L. Marsicano,<sup>4</sup> V. A. Matveev,<sup>6</sup> Yu. V. Mikhailov,<sup>9</sup> L. Molina Bueno,<sup>3,17</sup> D. V. Peshkxonov,<sup>6</sup> V. A. Polyakov,<sup>9</sup> B. Radics,<sup>3</sup> A. Rubbia,<sup>3</sup> K. M. Salamatin,<sup>6</sup> V. D. Samoylenko,<sup>9</sup> H. Sieber,<sup>3</sup> D. Shchukin,<sup>12</sup> O. Soto,<sup>18,15</sup> V. O. Tikhomirov,<sup>12</sup> I. V. Tlisova,<sup>1</sup> A. N. Toropin,<sup>1</sup> B. I. Vasilishin,<sup>7</sup> P. V. Volkov,<sup>6,16</sup> V. Yu. Volkov,<sup>16</sup> I. Voronchikhin,<sup>7</sup> and J. Zamora-Saá<sup>14,15</sup>

(The NA64 Collaboration)

<sup>1</sup>*Institute for Nuclear Research, 117312 Moscow, Russia*

<sup>2</sup>*CERN, European Organization for Nuclear Research, CH-1211 Geneva, Switzerland*

<sup>3</sup>*ETH Zürich, Institute for Particle Physics and Astrophysics, CH-8093 Zürich, Switzerland*

<sup>4</sup>*INFN, Sezione di Genova, 16147 Genova, Italia*

<sup>5</sup>*Università degli Studi di Genova, 16126 Genova, Italy*

<sup>6</sup>*Joint Institute for Nuclear Research, 141980 Dubna, Russia*

<sup>7</sup>*Tomsk Polytechnic University, 634050 Tomsk, Russia*

<sup>8</sup>*UCL Department of Physics and Astronomy, University College London, Gower St. London WC1E 6BT, United Kingdom*

<sup>9</sup>*State Scientific Center of the Russian Federation Institute for High Energy Physics of National Research Center 'Kurchatov Institute' (IHEP), 142281 Protvino, Russia*

<sup>10</sup>*Physics Department, University of Patras, 265 04 Patras, Greece*

<sup>11</sup>*Technische Universität München, Physik Department, 85748 Garching, Germany*

<sup>12</sup>*P.N.Lebedev Physical Institute of the Russian Academy of Sciences, 119 991 Moscow, Russia*

<sup>13</sup>*Universität Bonn, Helmholtz-Institut für Strahlen-und Kernphysik, 53115 Bonn, Germany*

<sup>14</sup>*Center for Theoretical and Experimental Particle Physics, Facultad de Ciencias Exactas, Universidad Andres Bello, Fernandez Concha 700, Santiago, Chile*

<sup>15</sup>*Millennium Institute for Subatomic Physics at High-Energy Frontier (SAPHIR), Fernandez Concha 700, Santiago, Chile*

<sup>16</sup>*Skobeltsyn Institute of Nuclear Physics, Lomonosov Moscow State University, 119991 Moscow, Russia*

<sup>17</sup>*Instituto de Fisica Corpuscular (CSIC/UV), Carrer del Catedratic José Beltrán Martínez, 2, 46980 Paterna, Valencia*

<sup>18</sup>*Departamento de Física, Facultad de Ciencias,*

*Universidad de La Serena, Avenida Cisternas 1200, La Serena, Chile*

(Dated: October 25, 2022)

A search for a new  $Z'$  gauge boson associated with (un)broken  $B - L$  symmetry in the keV-GeV mass range is carried out for the first time using the missing-energy technique in the NA64 experiment at the CERN SPS. From the analysis of the data with  $3.22 \times 10^{11}$  electrons on target collected during 2016 - 2021 runs no signal events were found. This allows to derive new constraints on the  $Z' - e$  coupling strength, which for the mass range  $0.3 \lesssim m_{Z'} \lesssim 100$  MeV are more stringent compared to those obtained from the neutrino-electron scattering data.

Models with the gauged difference between baryon and lepton number,  $B - L$ , are attractive and well-motivated extensions of the standard model (SM) [1, 2] that may explain two of the most challenging problems in particle physics today - the origin of neutrino masses [3] -[7] and the nature of dark matter (DM) [8]-[17]. They could

also serve as an explanation for several existing experimental anomalies, such as e.g. an excess of low energy events recently observed by XENON1T [18–20]. Among the possible realizations of such models, the minimal one is based on the gauge group  $SU(2)_L \times U(1)_Y \times U(1)_{B-L}$ , which simply extends the SM with an extra  $U(1)$  gauge group associated to the difference of baryon number  $B$  and lepton number  $L$ . In these models, the cancellation of gauge anomalies is usually achieved by adding three right-handed neutrinos, which simultaneously allow

\* Corresponding author; Sergei.Gninenko@cern.ch

to explain neutrino masses via the type-I seesaw mechanism. Below, we consider two cases of  $B-L$  extensions of the SM, with unbroken and spontaneously broken  $B-L$  symmetry. The  $B-L$  gauge coupling  $g_{B-L}$  in these models can be small and the associated gauge boson  $Z'$  could have a mass well below the electroweak scale ( $\ll 100$  GeV), see e.g. [21–23]. Searches for new physics at such a low energy scale recently received significant attention from the community, see e.g. [24–26].

In addition to Dirac neutrinos, an unbroken  $U(1)_{B-L}$  brings with it only one more particle: the gauge boson  $Z'$ , coupled to the  $B-L$  current  $j_{B-L} = j_B - j_L$  via  $g_{B-L} Z'_\mu j_{B-L}^\mu$ , and leading to the Lagrangian:

$$\mathcal{L} \supset g_{B-L} Z'_\mu \sum_{families} \left[ \frac{1}{3} \bar{q} \gamma^\mu q - \bar{l} \gamma^\mu l - \bar{\nu} \gamma^\mu \nu \right] \quad (1)$$

where the  $g_{B-L}$  is the  $U(1)_{B-L}$  coupling constant, and  $q$ ,  $l$  and  $\nu$  are quark, charged lepton and neutrino fields, respectively. The  $Z'$  can kinetically mix with the hypercharge boson [27], effectively coupling it to the hypercharge current. We will neglect this kinetic mixing in the following for simplicity.

For comparison with the unbroken  $B-L$ , we will also consider the case of the spontaneously broken  $B-L$  symmetry. The neutrino sector of such gauge  $B-L$  model consists of three heavy ( $N_i$ ) and three light Majorana neutrinos. The  $N_i$  could be a viable DM candidate explaining the relic density via the freeze-out mechanism with a mass lying in the range including the keV to TeV scale, see, e.g. [28].

If the light  $Z'$  boson exists, crucial questions about its mass scale, coupling constants, decay modes, etc. arise, providing an important target for the  $(m_{Z'}, g_{B-L})$  parameter space, which can be probed at energies attainable at accelerators. One possible way to answer these questions is to search for  $Z'$  in neutrino-electron scattering experiments. The  $Z'$  signature would be an observation of an excess of recoil electrons in neutrino-electron scattering due to nonstandard  $\nu-e$  interaction transmitted by the  $Z'$ . The signal event rate in the detector in this case scales as  $\sim \frac{g_{B-L}^4 Z m_e E_\nu}{m_{Z'}^4}$ , where  $g_{B-L}$ ,  $m_e$ ,  $E_\nu$  are the  $Z'$  coupling strength, the mass of electron, and the neutrino energy, respectively, and  $Z$  is the charge of the target nuclei. Recently, severe limits on the  $B-L$   $Z'$  excluding the coupling strength range  $10^{-6} \lesssim g_{B-L} \lesssim 10^{-2}$  have been obtained for the masses  $1 \text{ keV} \lesssim m_{Z'} \lesssim 1 \text{ GeV}$  [19, 29, 30] from the results of neutrino-electron scattering experiments, such as TEXONO [31–33] and GEMMA [34] at nuclear reactors, BOREXINO [35] using solar neutrinos, LSND [36], and CHARM II [37] at neutrino beams from accelerators, leaving, however, a significant area of the parameter space still unexplored.

Another approach, considered in this work was proposed in Refs. [38–41]. It is based on the searches for invisible  $Z'$  in missing energy events from the reaction chain  $e^- Z \rightarrow e^- Z Z'$ ;  $Z' \rightarrow \nu\nu$  of the bremsstrahlung  $Z'$  production in high-energy electron scattering off

heavy nuclei of an active beam-dump and its subsequent prompt invisible decay into a neutrino pair. The advantage of this type of experiment compared to the neutrino-scattering is that its sensitivity is proportional to the square of the ratio of the  $Z'$  coupling strength to its mass,  $(\frac{g_{B-L} Z}{m_{Z'}})^2$ , associated with the  $Z'$  production in the primary reaction. In the former case, for  $m_{Z'} \gg E_\nu$  and couplings  $g_{B-L} \ll 1$ , it is significantly suppressed by the additional factor  $(g_{B-L}/m_{Z'})^2$ , associated with the  $Z'$  mediating the  $\nu-e$  interaction.

As the  $Z'$  boson couples to any fermion  $f_i$  including the heavy neutrino  $N_i$ , the total decay width of  $Z'$  is defined by the sum  $\Gamma_{tot}(Z') = \sum_i \Gamma_i(Z' \rightarrow f_i \bar{f}_i)$  over the leptonic invisible  $\Gamma(Z' \rightarrow \nu_i \nu_i, N_i, N_i)$  and visible  $\Gamma(Z' \rightarrow e^+ e^-, \mu^+ \mu^-)$ , and hadronic  $\Gamma(Z' \rightarrow q_i \bar{q}_i)$  final states. The decay rate into a leptonic pair is given by

$$\Gamma_l(Z') = \frac{1}{3} \alpha_{B-L} m_{Z'} \left( 1 + 2 \frac{m_l^2}{m_{Z'}^2} \right) \left( 1 - 4 \frac{m_l^2}{m_{Z'}^2} \right)^{1/2} \quad (2)$$

Here,  $\alpha_{B-L} = \frac{g_{B-L}^2}{4\pi}$ . For the model with unbroken  $U(1)_{B-L}$ , the invisible width of  $Z'$  is then determined by its decay into the three light Dirac neutrinos  $\nu = \nu_L + \nu_R$ ,  $\Gamma_{inv}(Z') = 3\Gamma(Z' \rightarrow \bar{\nu}\nu) = \alpha_{B-L} m_{Z'}$ , which effectively counts the number of light neutrinos. For the broken  $U(1)_{B-L}$  case, in addition to the  $Z' \rightarrow \nu\nu$  decays to light Majorana neutrinos, three invisible decays of  $Z'$  to heavy Majorana neutrinos contribute assuming the  $m_{Z'} > 2m_{N_i}$  case with the rate

$$\Gamma_{inv}(Z' \rightarrow N_i N_i) = \frac{1}{6} \alpha_{B-L} m_{Z'} \left( 1 - 4 \frac{m_{N_i}^2}{m_{Z'}^2} \right)^{3/2} \quad (3)$$

In the mass range  $m_{Z'} < 0.7$  GeV relevant for this

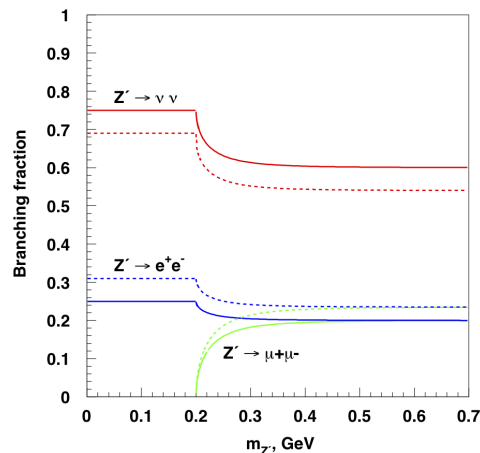


FIG. 1.  $Z'$  decay branching ratios to  $\nu_i \nu_i$ ;  $N_i N_i$  (red),  $e^+ e^-$  (blue), and  $\mu^+ \mu^-$  (green) for the unbroken (solid line) and broken (dashed line)  $U(1)_{B-L}$  models. See text for details.

work, the  $Z'$  decays mostly invisibly with the contributions from the visible decay modes  $Z' \rightarrow e^+ e^-, \mu^+ \mu^-$

the partial widths of which are shown in Fig. 1. Here for simplicity, three degenerate heavy neutrino species with the mass ratio  $\frac{m_{N_i}}{m_{Z'}} = \frac{1}{3}$  used for calculation of the phase space factor in (3) have been assumed.

In this Letter we report new results on the search for the  $Z'$  in the NA64 fixed-target experiment at the CERN SPS. The experiment employed the optimized H4 100 GeV electron beam with a maximal intensity  $\simeq 10^7$  electrons per SPS spill of 4.8 s produced by the primary 400 GeV proton beam. The detector used the beam scintillator and veto counters, a magnetic spectrometer consisting of two successive dipole magnets MBPL and a low-material-budget tracker. The tracker was a set of micromegas (MM), straw-tube (ST) and GEM chambers allowing the measurements of  $e^-$  momenta with the precision  $\delta p/p \simeq 1\%$  [42, 43]. Synchrotron radiation (SR) emitted in the MBPL magnetic field was used for efficient tagging of beam electrons with a SR detector (SRD) [38, 44], providing powerful suppression of the initial hadron contamination in the beam  $\pi/e^- \lesssim 10^{-2}$  down to the level  $\simeq 10^{-5}$ . The detector was also equipped with an active target, which was an electromagnetic calorimeter (ECAL), a matrix of Shashlik-type modules for measurement of the electron energy  $E_{ECAL}$ . Each module has  $\simeq 40$  radiation lengths ( $X_0$ ) with the first  $4X_0$  used as a preshower detector. Downstream of the ECAL, the detector was equipped with a large veto counter VETO, and a hadronic calorimeter (HCAL) of  $\simeq 30$  nuclear interaction lengths. The HCAL served as an efficient veto to detect muons and hadronic secondaries produced in the  $e^-A$  interactions in the target. The events were collected with a beam defining trigger requiring, also, an in-time cluster in the ECAL with the energy  $E_{ECAL} \lesssim 80$  GeV. More detail of the NA64 detector can be found in [45–47].

The search described in this paper uses the data samples of  $n_{EOT} = 3.22 \times 10^{11}$  electrons on target (EOT), collected in the years 2016, 2017, 2018 [45–48] and 2021 with the beam intensities mostly in the range  $\simeq (5 - 6) \times 10^6$   $e^-$  per spill. Data from these four runs (hereafter called respectively runs I,II, III, and IV) were processed with selection criteria similar to the one used in Refs. [46, 47] and, finally, combined as described below. Compared to the 2016-2018 runs, in the 2021 run the ECAL target and the HCAL were moved upstream to increase the detector coverage resulting in a significant reduction of background from large-angle secondaries from the  $e^-$  hadronic interactions in the beam line.

A detailed GEANT4 [49, 50] based Monte Carlo (MC) simulation was used to study the signal acceptance and backgrounds, and optimize selection criteria. For calculations of the signal yield we used the fully GEANT4 compatible package DMG4 [51]. Using this package the production of  $Z'$  in the process  $e^-Z \rightarrow e^-ZZ'$ ;  $Z' \rightarrow \nu\nu$  has been simulated with the cross sections obtained from the exact tree-level calculations, see, e.g., Refs. [40, 41].

The number  $dn_{Z'}(m_{Z'}, E_{Z'}, E_0)$  of produced  $Z'$  bosons with a given mass  $m_{Z'}$  and energy  $E_{Z'}$  per single EOT

with the energy  $E_0$  was obtained from

$$\frac{dn_{Z'}}{dE_{Z'}} = \frac{\rho N_A}{A_{Pb}} \int_0^T \int_0^{E_0} n(E_0, E_e, s) \frac{d\sigma_{Z'}(E_e)}{dE_{Z'}} dE_e ds \quad (4)$$

where  $\rho$  is density of the target,  $N_A$  is the Avogadro's number,  $A_{Pb}$  is the Pb atomic mass,  $n(E_0, E_e, s)$  is the number of  $e^\pm$  in the  $e$ - $m$  shower at the depth  $s$  (in radiation lengths) with energy  $E_e$  within the target of total thickness  $T$ , and  $\frac{d\sigma_{Z'}(E_e)}{dE_{Z'}}$  is the differential cross section for the  $Z'$  production in the reaction  $e^-Z \rightarrow e^-ZZ'$  via the interaction of Eq.(1) in the kinematically allowed region up to  $Z'$  energies  $E_{Z'} \simeq E_e$  by an electron with the energy  $E_e$ . It depends, in particular, on the coupling and mass  $g_{B-L}$ ,  $m_{Z'}$ , and the beam energy  $E_0$ . The efficiency of  $e^-Z \rightarrow e^-ZZ'$ ;  $Z' \rightarrow \nu\nu$  event registration in our detector was also cross-checked by reconstructing the rare QED processes of dimuon production,  $e^-Z \rightarrow e^-Z\gamma$ ;  $\gamma \rightarrow \mu^+\mu^-$ . These events, dominated by the ECAL shower photons conversion into  $\mu^+\mu^-$  pairs on a target nucleus, are similar to the  $Z' \rightarrow \nu\nu$  decay events if the energy deposition in the HCAL is requested to be above the two minimum ionizing particle threshold. The dimuon production was used as a benchmark process allowing us to verify the reliability of simulations, systematic uncertainties and background estimations [46, 47].

A blind analysis similar to the one described in Ref.[47] was performed by using the following selection criteria: (i) The beam track momentum should be within  $100 \pm 3$  GeV; (ii) The energy detected by the SRD should be consistent with the SR energy emitted by  $e^-$ 's in the magnets; (iii) The shower shape in the ECAL should be as expected from the signal-event shower [40]; (iv) A single track should be reconstructed in the tracker chambers upstream of the ECAL; and (v) There should be no activity in the VETO.

In the 2021 run the main background faking the signal of  $e^-Z \rightarrow e^-ZZ'$  from the hadronic interactions of the  $e^-$  beam in the beam line materials accompanied by the emission of hadronic secondaries at a large-angle (high  $p_T$ ) was more suppressed compared to the 2016-2018 runs due to the improved detector coverage. By selecting events with no additional tracks or hits in MM and ST chambers upstream and downstream of the magnets, most of events with charged hadronic secondaries were rejected. The remaining background of  $0.03 \pm 0.015$  events from large angle secondary neutrals was evaluated directly from the data by the extrapolation of events from the sideband ( $E_{ECAL} > 50$  GeV;  $E_{HCAL} < 1$  GeV) (region  $C$  in Fig.2) into the signal region and estimating the systematic errors by varying the fit functions as described in Ref. [46]. Another background from region  $A$  in Fig.2, mostly from punch through of leading neutral hadrons ( $n, K_L^0$ ) with energy  $\gtrsim 0.5 E_0$  produced by the beam  $e^-$ 's in the target, was evaluated from the study of their propagation through the HCAL modules [48] and was found to be negligible. Other sources of background such as loss of dimuons and decays in flight of beam  $\pi$ ,

$K$ , were simulated and were also found to be negligible.

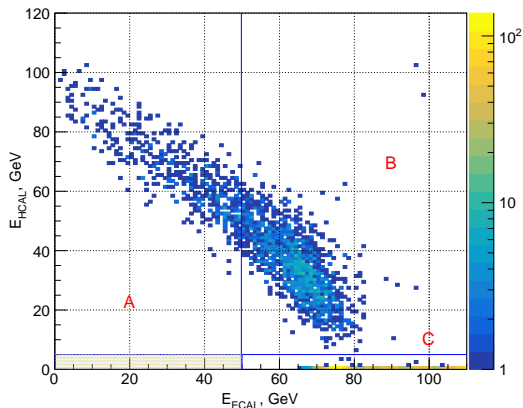


FIG. 2. The energy distribution of events in the  $E_{\text{ECAL}}; E_{\text{HCAL}}$  plane selected from the data sample of the 2021 run collected with intensity  $\simeq 5 \times 10^6 e^-$  per spill after applying all selection criteria. The shaded area is the signal box, which contains no events. The size of the signal box along the  $E_{\text{HCAL}}$  axis is increased by a factor of 5 for illustration.

The overall signal efficiency  $\epsilon_{Z'}$ , which includes efficiencies for the geometrical acceptance, the track, SRD, VETO and HCAL selections and the DAQ dead time, was found to be slightly  $m_{Z'}$  dependent [47]. The ECAL signal selection efficiency,  $\epsilon_{\text{ECAL}}$ , was estimated for different  $Z'$  masses. The  $\epsilon_{\text{ECAL}}$  value for a shower from a  $Z'$  event has to be corrected compared to the ordinary  $e-m$  shower, due to differences in the development of the  $e-m$  showers at the early stage in the ECAL preshower (PS) [40]. This correction was  $\lesssim (5 \pm 3)\%$ , depending on the energy threshold in the PS ( $E_{\text{PS}}^{\text{th}}$ ) used in the trigger. The systematic uncertainty is dominated by the  $E_{\text{PS}}^{\text{th}}$  variation during the run, mostly due to the instabilities in the photomultiplier gains. The VETO and HCAL selection efficiencies are defined by the noises, pile up and the leakage of the signal shower energy from the ECAL to these detectors. They were studied using the electron calibration runs and simulations. The uncertainty in the efficiencies estimated to be  $\lesssim 4\%$  is dominated mostly by the pile up effect. The total signal selection efficiency with all criteria used except ECAL threshold on missing energy varied from  $\sim 0.62$  to  $\sim 0.48$  with the uncertainty in the signal yield to be  $\simeq 10\%$  [46].

Data from runs I-IV were analyzed simultaneously using the multibin limit setting [46] technique, with the code based on the RooStats package [52]. The signal box ( $E_{\text{ECAL}} < 50 \text{ GeV}; E_{\text{HCAL}} < 1 \text{ GeV}$ ) was defined based on the energy spectrum calculations for  $Z'$  bosons emitted by  $e^\pm$  from the  $e-m$  shower generated by the primary  $e^-$ s in the ECAL [40, 41] and the HCAL zero-energy threshold determined mostly by the noise of the readout electronics. The size of the signal box was optimized by comparing sensitivities defined as an average expected

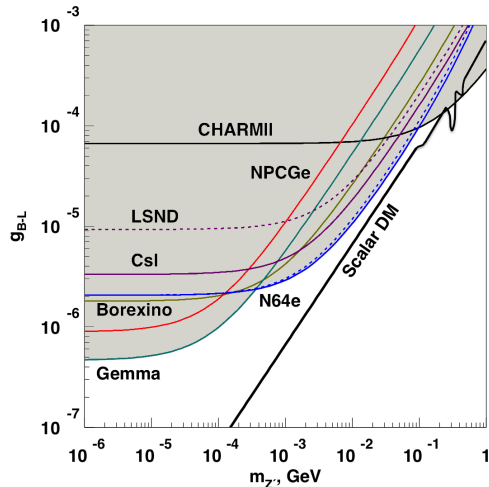


FIG. 3. The NA64 90% C.L. exclusion region in the  $(m_{Z'}, g_{B-L})$  plane for the unbroken (solid blue line) and broken (dashed blue line)  $U(1)_{B-L}$ . For the latter case, three degenerate heavy neutrino species with the mass ratio  $\frac{m_{N_i}}{m_{Z'}} = \frac{1}{3}$  have been assumed. Constraints from the results of neutrino-electron scattering experiments obtained with nuclear-reactor neutrinos at TEXONO [31–33] and GEMMA [34], solar neutrinos at BOREXINO [35], and accelerator neutrino beams at LSND [36], and CHARM II [37] derived in Refs. [19, 29] are also shown. The dashed area above the curves is excluded. As an example, the black curve illustrates the parameter space for the thermal scalar DM model for which the abundance of scalar  $\chi$  is in agreement with the observed DM energy density. The curve is calculated assuming the  $Z' - \chi$  coupling  $\alpha_D = 0.1$  and the mass ratio  $m_{Z'} = 3m_\chi$ , see Ref.[57].

limit calculated using the profile likelihood method. It was found weakly dependent on the  $Z'$  mass and was finally set to  $E_{\text{ECAL}} \lesssim 50 \text{ GeV}$  for all four runs and the whole mass range. The uncertainties in the signal yield and background level were treated as nuisance parameters in the statistical model [53].

The total number of signal events in the signal box was the sum of events expected from each of the four runs:

$$N_{Z'} = \sum_{j=1}^4 n_{\text{EOT}}^j \epsilon_{Z'}^j n_{Z'}^j(g_{B-L}, m_{Z'}, \Delta E_{Z'}) \quad (5)$$

where  $\epsilon_{Z'}^j$  is the signal efficiency in run  $j$ , and  $n_{Z'}^j(g_{B-L}, m_{Z'}, \Delta E_{Z'})$  is the signal yield per EOT generated in the energy range  $\Delta E_{Z'}$ . Each  $j$ th entry in Eq.(5) was calculated with simulations of signal events processing them through the reconstruction program with the same selection criteria and efficiency corrections as for the data sample from run  $j$ . The corresponding yield

$n_{Z'}^j$ , of  $Z' \rightarrow invisible$  events was defined by

$$n_{Z'}^j(g_{B-L}, m_{Z'}, \Delta E_{Z'}) = \int \frac{dn_{Z'}^j}{dE_{Z'}} [Br(Z' \rightarrow \nu\nu) + (6) \\ + \sum_{l=e,\mu} Br(Z' \rightarrow l^+l^-) e^{-\frac{L_{\text{ECAL}}+L_{\text{HCAL}}}{L_{Z'}}}] dE_{Z'}$$

where  $\frac{dn_{Z'}^j}{dE_{Z'}}$  was calculated with Eq.(4), and the term in square brackets gives the probability for the produced  $Z'$  with a given mass  $m_{Z'}$  and energy  $E_{Z'}$ , to make a transition into the invisible final state, i.e. to decay either into  $\nu\nu$  pair, or outside the HCAL modules into a  $e^+e^-$  or  $\mu^+\mu^-$  pair. Here,  $Br(Z' \rightarrow \nu\nu)$  varies in the range 0.6 - 0.75, depending on  $m_{Z'}$ , see Fig. 1,  $L_{Z'} = \frac{c\tau_{Z'} E_{Z'}}{m_{Z'}}$  and  $L_{\text{ECAL}}+L_{\text{HCAL}}$  are the  $Z'$  decay length and the total length of the ECAL + HCAL detectors, respectively, and  $\tau_{Z'} = \frac{1}{\Gamma_{\text{tot}}(Z')}$  is the lifetime of the  $Z'$ . After determining all selection criteria, background level, systematic uncertainties, we open the box and found 0 events, as shown in the left panel of Fig. 2, consistent with  $0.56 \pm 0.17$  events from the background estimations for the full data sample from the 2016-2018 [47] and 2021 runs.

The combined 90% CL exclusion limits on the coupling  $g_{B-L}$  as a function of the  $Z'$  mass, calculated using the modified frequentist approach [47, 54–56] for the models with unbroken and broken  $U(1)_{B-L}$  symmetry are shown in Fig. 3. For the latter case, three degenerate heavy neutrino species with the mass ratio  $\frac{m_{N_i}}{m_{Z'}} = \frac{1}{3}$  have been assumed. As an example, we also show the most motivated

region of the parameter space for the thermal scalar DM model, in which the  $Z'$  also mediates new feeble interaction between the SM and DM [57]. The treatment of the general case with other assumptions for the  $N_i$  masses is straightforward and does not qualitatively change our main conclusions. For example, if the  $m_{Z'} < 2m_{N_i}$  case is assumed, i.e. no  $Z'$  decays into heavy neutrinos, the  $Z'$  invisible branching ratio of  $Br(Z' \rightarrow \nu_i\nu_i; N_i N_i) \simeq 54\%$  shown in Fig. 1 drops to  $Br(Z' \rightarrow \nu_i\nu_i) \simeq 43\%$  and the corresponding limit for the mass range  $m_{Z'} \gtrsim 100$  MeV, see Fig. 3, will be  $\simeq 10\%$  worse. Finally, note that for the mass range  $0.3 \lesssim m_{Z'} \lesssim 100$  MeV, NA64 bounds are more stringent than those derived from the results of neutrino-electron scattering. Another advantage of the NA64 approach compared to neutrino experiments in the case of the signal observation is its potential capability to distinguish the unbroken and broken  $B-L$  scenarios by measuring the ratio  $\frac{Br(Z' \rightarrow invisible)}{Br(Z' \rightarrow e^+e^-)}$ , see Fig. 1.

We gratefully acknowledge the support of the CERN management and staff for their vital contributions. This work was supported by the Helmholtz-Institut für Strahlen-und Kernphysik (HISKP), University of Bonn (Germany), Joint Institute for Nuclear Research (JINR) (Dubna), the Ministry of Science and Higher Education (MSHE) and RAS (Russia), ETH Zurich and SNSF Grants No. 169133, No. 186181, No. 186158, No. 197346 (Switzerland), and FONDECYT Grants No.1191103, No. 190845 and ANID–Millennium Program – Grant No. ICN2019\_044 (Chile). We acknowledge the support of the European Research Council (ERC) under the European Union’s Horizon 2020 research and innovation programme, Grant No. 947715 (POKER).

- 
- [1] A. Davidson, Phys. Rev. D **20**, 776 (1979).  
[2] R.E. Marshak and R.N. Mohapatra, Phys. Lett. **91B**, 222 (1980).  
[3] P. Minkowski, Phys. Lett. **67B**, 421 (1977).  
[4] T. Yanagida, Conf. Proc. C **7902131**, 95 (1979).  
[5] M. Gell-Mann, P. Ramond, and R. Slansky, Conf. Proc. C **790927**, 315 (1979).  
[6] R.N. Mohapatra and G. Senjanovic, Phys. Rev. Lett. **44**, 912 (1980).  
[7] S.L. Glashow, NATO Sci. Ser. B **61**, 687 (1980).  
[8] S. Kanemura, T. Matsui, and H. Sugiyama, Phys. Rev. D **90**, 013001 (2014).  
[9] N. Okada and O. Seto, Phys. Rev. D **82**, 023507 (2010).  
[10] N. Okada and Y. Orikasa, Phys. Rev. D **85**, 115006 (2012).  
[11] L. Basso, O. Fischer, and J.J. van der Bij, Phys. Rev. D **87**, 035015 (2013).  
[12] T. Basak and T. Mondal, Phys. Rev. D **89**, 063527 (2014).  
[13] M. Lindner, D. Schmidt, and A. Watanabe, Phys. Rev. D **89**, 013007 (2014).  
[14] M. Duerr, P. Fileviez Perez, and J. Smirnov, Phys. Rev. D **92**, 083521 (2015).  
[15] J. Guo, Z. Kang, P. Ko, and Y. Orikasa, Phys. Rev. D **91**, 115017 (2015).  
[16] W. Rodejohann and C.E. Yaguna, J. Cosmol. Astropart. Phys **12**, (2015) 032.  
[17] R.N. Mohapatra and N. Okada, Phys. Rev. D **102**, 035028 (2020).  
[18] C. Boehm, D. G. Cerdeno, M. Fairbairn, P. A. N. Machado, and A. C. Vincent, Phys. Rev. D **102**, 115013 (2020).  
[19] M. Lindner, Y. Mambrini, T. B. de Melo, and F. S. Queiroz, Phys. Lett. B **811**, 135972 (2020).  
[20] G. Choi, T. T. Yanagida, and N. Yokozaki, Phys. Lett. B **810**, 135836 (2020).  
[21] J. Heeck, Phys. Lett. B **739**, 256 (2014).  
[22] M.D. Campos, D. Cogollo, M. Lindner, T. Melo, F. S. Queiroz, and W. Rodejohann, J. High Energy Phys. **08**, (2017) 092.  
[23] N. Okada, S. Okada, D. Raut, and Q.Shafi, Phys. Lett. B **810**, 135785 (2020).  
[24] M. Battaglieri *et al.*, arXiv:1707.04591.  
[25] J. Beacham *et al.*, J. Phys. G **47**, 010501 (2020).  
[26] P. Agrawal *et al.*, Eur. Phys. J. C **81**, 1015 (2021).  
[27] B. Holdom, Phys. Lett. **166B**, 196 (1986).  
[28] K. Kaneta, Zh. Kang, and H.-S. Lee, JHEP **02**, 031 (2017).

- [29] S. Bilmis, I. Turan, T. M. Aliev, M. Deniz, L. Singh, and H. T. Wong, Phys. Rev. D **92**, 033009 (2015).
- [30] M. Lindner, F. S. Queiroz, W. Rodejohann, and Xun-Jie Xu, J. High Energy Phys. **05**, (2018) 098.
- [31] M. Deniz *et al.*, Phys. Rev. D **81**, 072001 (2010).
- [32] H. B. Li *et al.*, Phys. Rev. Lett. **90**, 131802 (2003); Phys. Rev. D **75**, 012001 (2007).
- [33] J.-W. Chen, H.-C. Chi, H.-B. Li, C.-P. Liu, L. Singh, H. T. Wong, C.-L. Wu, and C.-P. Wu, Phys. Rev. D **90**, 011301(R) (2014).
- [34] A. G. Beda, E. V. Demidova, A. S. Starostin, V. B. Brudanin, V. G. Egorov, D. V. Medvedev, M. V. Shirchenko, and T. Vylov, Phys. Part. Nucl. Lett. **7**, 406 (2010).
- [35] G. Bellini *et al.*, Phys. Rev. Lett. **107**, 141302 (2011).
- [36] L.B. Auerbach *et al.*, Phys. Rev. D **63**, 112001 (2001).
- [37] P. Vilain *et al.*, Phys. Lett. B **302**, 351 (1993); **335**, 246 (1994).
- [38] S. N. Gninenko, Phys. Rev. D **89**, 075008 (2014).
- [39] S. Andreas *et al.*, arXiv:1312.3309.
- [40] S. N. Gninenko, N. V. Krasnikov, M. M. Kirsanov, and D. V. Kirpichnikov, Phys. Rev. D **94**, 095025 (2016).
- [41] S. N. Gninenko, D. V. Kirpichnikov, M. M. Kirsanov, and N. V. Krasnikov, Phys. Lett. B **782**, 406 (2018).
- [42] D. Banerjee, P. Crivelli, and A. Rubbia, Adv. High Energy Phys. **2015**, 105730 (2015).
- [43] V.Yu. Volkov *et al.*, Phys. Part. Nucl. Lett. **16**, 847(2019).
- [44] E. Depero *et al.*, Nucl. Instrum. Methods. Phys. Res., Sect. A **866**, 196 (2017).
- [45] D. Banerjee *et al.* (NA64 Collaboration), Phys. Rev. Lett. **118**, 011802 (2017).
- [46] D. Banerjee *et al.* (NA64 Collaboration), Phys. Rev. D **97**, 072002 (2018).
- [47] D. Banerjee *et al.* (NA64 Collaboration), Phys. Rev. Lett. **123**, 121801 (2019).
- [48] D. Banerjee *et al.* (NA64 Collaboration), Phys. Rev. Lett. **125**, 081801 (2020).
- [49] S. Agostinelli *et al.* [GEANT4 Collaboration], Instrum. Methods Phys. Res., Sect. **506**, 250 (2003).
- [50] J. Allison *et al.*, IEEE Trans. Nucl. Sci. **53**, 270 (2006).
- [51] M. Bondi, A. Celentano, R. R. Dusaev, D. V. Kirpichnikov, M. M. Kirsanov, N. V. Krasnikov, L. Marsicano, and D. Shchukin, Comput. Phys. Commun. **269**, 108129 (2021).
- [52] L. Moneta *et al.*, Proc. Sci. ACAT2010, (2010) 057.
- [53] E. Gross, Report No. CERN-2008-001, CERN, 2008, p.71.
- [54] T. Junk, Nucl. Instrum. Methods Phys. Res., Sect. **434**, 435 (1999).
- [55] G. Cowan, K. Cranmer, E. Gross, and O. Vitells, Eur. Phys. J. C **71**, 1554 (2011).
- [56] A. L. Read, J. Phys. G **28**, 2693 (2002).
- [57] A. Berlin, N. Blinov, G. Krnjaic, P. Schuster, and N. Toro, Phys. Rev. D **99**, 075001 (2019).